nature plants

ARTICLES

PUBLISHED: 2 MARCH 2015 | ARTICLE NUMBER: 15014 | DOI: 10.1038/NPLANTS.2015.14

Patterning mechanisms of cytoskeletal and cell wall systems during leaf trichome morphogenesis

Makoto Yanagisawa[1], Anastasia S. Desyatova[2], Samuel A. Belteton[1], Eileen L. Mallery[1], Joseph A. Turner[2] and Daniel B. Szymanski[1,3]*

The plant actin cytoskeleton is an unstable network of filaments that influences polarized growth through poorly understood mechanisms. Here, we used a combination of live cell imaging and finite element computational modelling of *Arabidopsis* trichome morphogenesis to determine how the actin and microtubule cytoskeletons cooperate to pattern the cell wall and growth. The actin-related protein (ARP)2/3 complex generates an actin meshwork that operates within a tip-localized, microtubule-depleted zone to modulate cell wall anisotropy locally. The actin meshwork also positions an actin bundle network that organizes organelle flow patterns. This activity is required to maintain cell wall thickness gradients that enable tip-biased diffuse growth. These newly discovered couplings between cytoskeletal patterns and wall textures provide important insights into the cellular mechanism of growth control in plants.

The microtubule and actin cytoskeletons cooperate to influence shape change in both metazoan[1] and plant[2] cells. In plants, these cytoskeletal systems locally modulate the mechanical properties of the cell wall[3,4], and in the epidermis, heterogeneities in wall texture guide the complex patterns of irreversible cell expansion[5]. In leaves, these growth patterns are important because they can persist for days[6,7] and influence organ size and shape[8]. Microtubule-dependent cellulose microfibril patterning is one central feature of polarized diffuse growth[9,10]; however, the means by which the actin and microtubule cytoskeletons cooperate during cell morphogenesis is poorly understood.

Leaf trichomes, specialized leaf epidermal cells that protect the growing organ against insect attack[11], like single-celled cotton fibres[12], are model cell types that can be used to analyse how the microtubule and actin cytoskeletons control polarized growth[13,14]. The *distorted Arabidopsis* leaf trichome mutants identified an evolutionarily conserved actin filament nucleation pathway, in which the WAVE/SCAR regulatory complex (W/SRC)[15] positively regulates the actin filament nucleator ARP2/3[16–18]. Although it is known that W/SRC–ARP2/3 is required to maintain organized actin bundle networks and polarized cell elongation[13,17,19–21], the mechanisms by which it influences the cell wall properties that determine the growth behaviours of the cell are not known. Here we integrate live cell imaging and computational analyses of the cell wall to determine how an ARP2/3-generated apical actin meshwork influences cell wall properties that define the geometry of shape change.

Creation of a plausible finite element model

Branch elongation and tip refinement are defining features of trichome morphogenesis[13], but at present there are no clear hypotheses about what combinations of cell wall mechanical properties would be needed to generate this type of shape change. Finite element computational modelling is a useful framework to simulate the complex relationships between turgor pressure, cell wall mechanical properties and growth[4]. To parameterize a finite element model of the cell wall and branch elongation, we conducted a series of reflected light time-lapse imaging experiments (Supplementary Fig. 1 and Supplementary Movie 1). Branch diameter at the base was nearly constant during growth, as would be expected for tip growth[4]. Unlike the tip growth of pollen tubes and root hairs in which the tip radius is quite constant, the radius of curvature at the tip decreased from ~4 μm to ~0.5 μm as the branch elongated (Fig. 1a,b). Branch growth rates varied considerably during morphogenesis (Supplementary Fig. 1b), but there was a general trend towards higher elongation rates as the branches increased in length. For example, short branches between 20 and 30 μm elongated at a rate of 3.1 ± 1.0 μm h^{-1}, which was significantly less than the growth rate of branches in the 50–60 μm range, which was 5.8 ± 1.5 μm h^{-1} ($P = 0.003$). On the basis of the shape change that occurs and on direct measurements of wall strain using cell wall bound pariticles[13,22], it is known that trichome morphogenesis includes a diffuse growth component. To measure wall strain patterns directly at high spatial resolution, externally applied fluorescent beads were used as fiducial marks along the branch axis (Fig. 1c). Particle tracking of bead pairs detected an axial strain gradient, in which distal regions of the branch grew at significantly faster rates than the branch base (Fig. 1d). Therefore, the early stages of branch elongation include highly polarized anisotropic diffuse growth and tip refinement to a final radius of 0.61 ± 0.12 μm ($n = 20$). Our analysis captured the significant shape change during branch development because mature branches that exceed 200 μm in length have similar length to width aspect ratios and tip geometry[13].

Organized microtubules and cellulose microfibrils are required for polarized branch growth[10,13,14]. To quantify the degree of potential microtubule-based microfibril ordering, we measured the microtubule angle distribution relative to the longitudinal axis of the cell (Fig. 1f). As expected, microtubules and the cellulose synthase (CESA) complex had a similar transverse alignment (Fig. 1e,g). However, the branch apex always contained an obvious microtubule-depleted zone (MDZ) that lacked patterned CESA localization. An MDZ has been previously reported in the literature using different microtubule markers[21,23], indicating that the branch apex wall has a more isotropic character than the flank.

[1]Department of Botany and Plant Pathology, Purdue University, West Lafayette, Indiana 47907, USA. [2]Department of Mechanical and Materials Engineering, University of Nebraska-Lincoln, Lincoln, Nebraska 68588, USA. [3]Biological Sciences, Purdue University, West Lafayette, Indiana 47907, USA. *e-mail: dszyman@purdue.edu

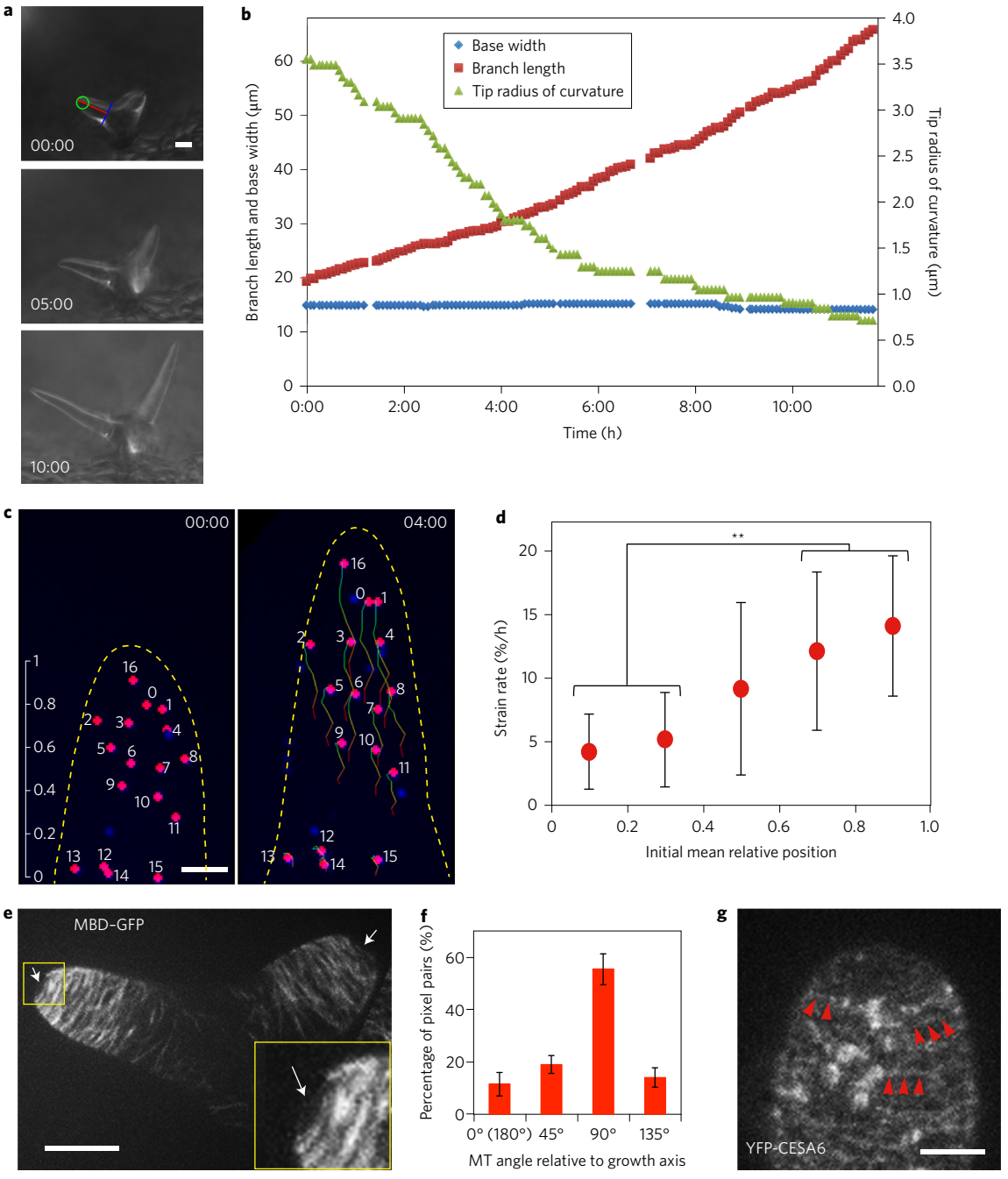

Figure 1 | The geometry of trichome shape change and cell wall strain. a, Reflected light time-lapse imaging of trichome morphogenesis. **b**, Branch length (red), base width (blue), and tip radius of curvature (green) plotted as a function of time for a representative wild-type branch. **c**, Local wall strain analysis using fluorescent beads. Projected image of the tracked bead movement over a 4 h time course. Yellow dashed lines indicate cell outlines. **d**, Strain rates as a function of normalized branch length with 0 corresponding to the base and 1 the branch tip. Values are mean ± s.d. ($n = 43$), $^{**}P < 0.01$ (Student t-test). **e**, Microtubule localization visualized with the MBD–GFP reporter. Inset is an enlarged view of the microtubule-binding domain (MDZ) at the branch apex. Arrows mark branch apex. **f**, Microtubule angle distributions with 90° defined as transverse to the growth axis. Values are mean ± s.d. ($n = 14$ cells). **g**, Yellow fluorescent protein (YFP)-CESA6 expressing trichome branch showing linearly aligned CESA6 marked with red arrowheads. Time stamps in **a** and **c** indicate hours:minutes. Scale bars, 10 μm in **a** and **e**; 5 μm in **c** and **g**.

Finite element modelling has been used to analyse the shape change of thin-walled pressurized plant cells[4], and can incorporate realistic material models of fibres reinforcing a matrix[24,25]. Spatial heterogeneities in the model were introduced by subdividing the shell from the tip to the base into multiple sections with varying properties (Fig. 2a and see Methods). Finite element simulations identified wall parameters that affected the rate of cell expansion and growth anisotropy (Supplementary Table 1). For example, the degree of fibre orientation strongly affected anisotropic expansion (Fig. 2b). The measured microtubule angle distributions (Fig. 1f) provided experimental support for highly ordered fibres with $\kappa = 0.141 \pm 0.029$, which could generate branches with the observed high length to width aspect ratios (Fig. 2b). Anisotropic branch expansion was also sensitive to the ratio of fibre to matrix elastic moduli (k_1/E_0) of the wall (Fig. 2c). A sensitivity analysis of the branch growth geometry to combinations of k_1/E_0 and κ parameters

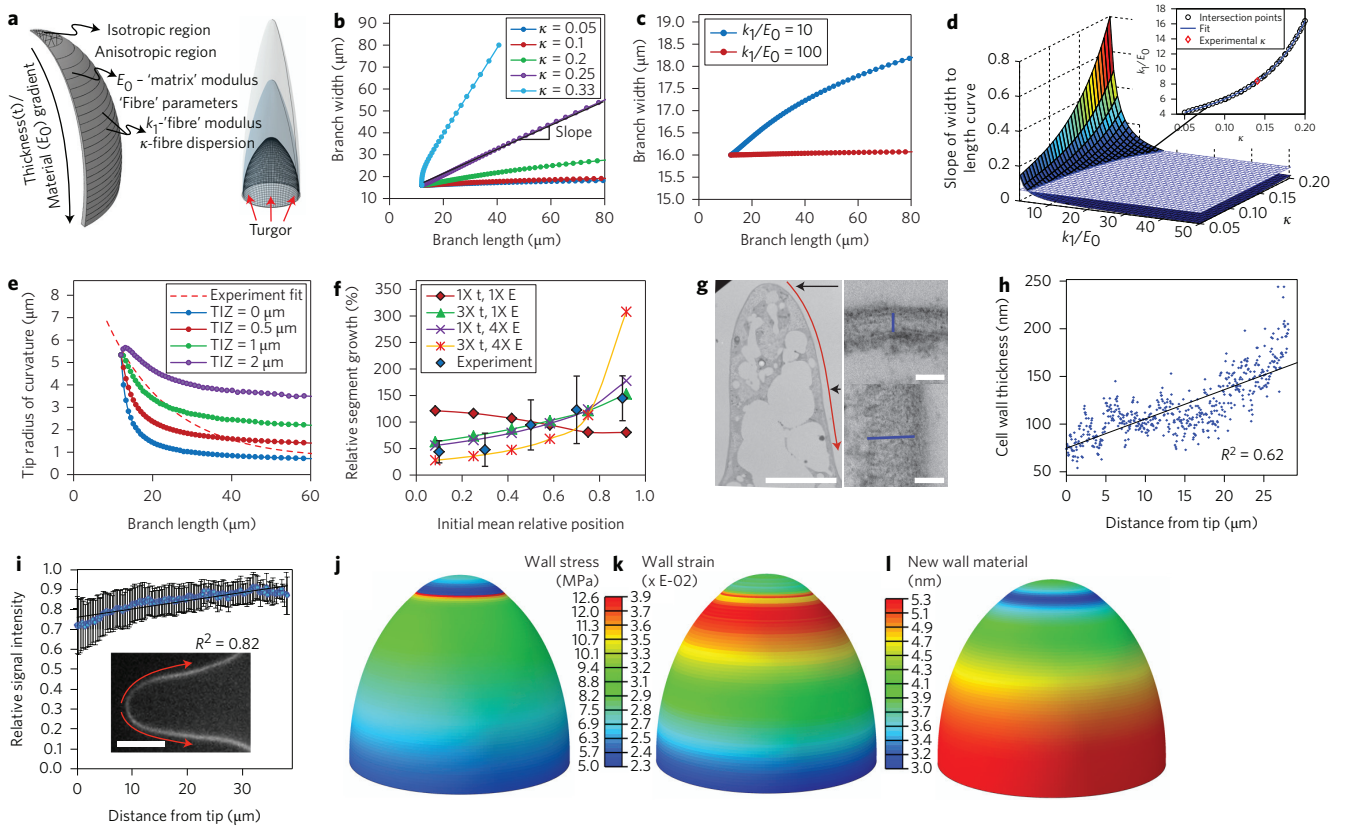

Figure 2 | Finite element model of trichome branch morphogenesis. a, Overview of the finite element model: key cell wall parameters (left) and example of trichome branch model growth (right). **b**,**c**, Sensitivity of the branch geometry during growth to fibre angular dispersion κ and fibre to matrix elastic moduli ratio k_1/E_0. **d**, Sensitivity map of the width to length slope to k_1/E_0 and κ (coloured surface) and its intersection with the observed branch width to length ratio (white plane). The insert shows the κ and k_1/E_0 relationship that led to the experimental aspect ratios. The red point represents experimental κ and the corresponding k_1/E_0. **e**, Effects of the TIZ size on the tip refinement. **f**, Effects of elastic modulus (E) and thickness (t) gradients on simulated wall strain patterns. *nX* represents the gradient value with *n* equal to the base value divided by the tip value. **g**,**h**, TEM measurements of wall thickness variation in developing wild-type trichome branches. Blue lines indicate cell wall thickness at branch locations marked by black arrows. **i**, Wall thickness analyses in a population of wild-type trichome branches using propidium iodide fluorescence quantification. Values are mean ± s.d. (n = 40). **j**,**k**, Wall von Mises stresses and maximum in-plane principal logarithmic strains. **l**, Cell wall synthesis spatial map, in terms of added thickness needed to restore wall thickness after one simulation cycle. Scale bars, 10 μm in left panel in **g** and **i**; 100 nm in right panels in **g**.

revealed the potential solution space (Fig. 2d). The experimentally observed values of branch width to length slope of 0.064 ± 0.026 and κ provided the value of k_1/E_0 = 8.4.

Importance of a tip isotropic zone and a thickness gradient

These combinations of k_1/E_0 and κ could reproduce the observed global aspect ratios of branch growth, but could not generate the reproducible patterns of tip refinement (Fig. 2e) and unequal axial strain (Fig. 2f) that were measured in the time-lapse analyses. Live cell measurements indicated that reductions in tip radius and MDZ size were highly correlated, and that the MDZ was efficiently centred on the branch axis (Fig. 3g,i), suggesting that an isotropic branch tip was involved in cell shape control. The finite element simulations showed that the trajectories of simulated tip refinement were very sensitive to the size of the tip isotropic zone (TIZ). Intermediate TIZs yielded better fits to the observed growth patterns; however, no single value performed the best for all simulation cycles (Fig. 2e). The modelling results and the coupled geometry of the MDZ and the branch tip radius of curvature suggest that the smooth progression of tip refinement includes modulation of the size of an apical cell wall domain with isotropic mechanical properties (see below). Finally, the observed apical to basal strain gradients that were detected in the bead labelling experiments (Fig. 1c,d) were studied. Finite element simulations that included fiducial marks could not reproduce the experimentally measured strain gradients unless a proximo-distal gradient was introduced in either elastic modulus or wall thickness (Fig. 2f).

These finite element simulations motivated experiments to quantify the predicted cell wall thickness gradient in trichome branches. First, wall thickness measurements were taken from transmission electron microscopy (TEM) images of medial longitudinal sections through young trichome branches (Fig. 2g). There were local variations in wall thickness; however, on the basis of an approximated linear relationship between cell wall thickness and distance from the branch tip, there was a positive correlation (Fig. 2h). The magnitude of the tip to base wall thickness gradient for the wild type was 2.49, and similar values were obtained in replicate TEM analyses of the adjacent wall of the same cell and the walls of another independent cell (Supplementary Fig. 2a–c). To increase our sample size and our confidence in the TEM results we used propidium iodide to quantify cell wall thickness variation[26]. The normalized propidium iodide signal was also correlated with distance from the branch tip (Fig. 2i). The propidium iodide variation was not caused by cell geometry effects at the image plane, because the signal of FM1-43, which labels the plasma membrane, had a negative correlation with distance from the tip (Supplementary Fig. 2d–g). Although pectin methyl esterification can affect propidium iodide staining in pollen tubes[27], the combined TEM and light microscopy

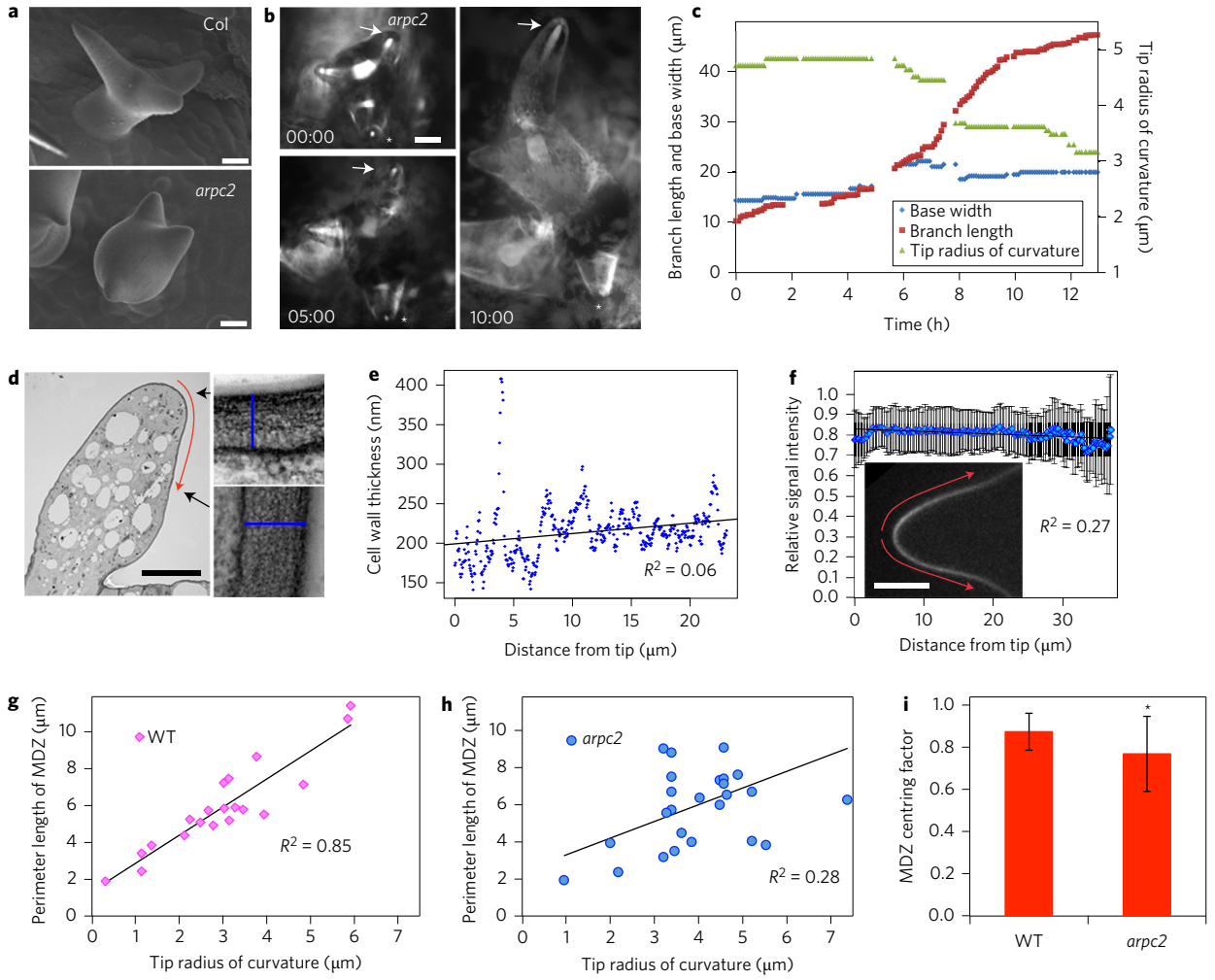

Figure 3 | Growth and cell wall analysis of an ARP2/3 null mutant. a, Scanning electron micrographs of wild type and *arpc2* trichomes with nascent branches. **b**, Time-lapse images of a soil-grown *arpc2* trichome with commonly observed growth phenotypes. Time stamps indicate hours:minutes. **c**, Plots of branch length (red), base width (blue), and tip radius of curvature (green) as a function of time from **b**. Gaps are present because at some time points one or more parameters could not be measured due to irregular growth patterns and poor image quality. **d**, Low and high magnification images of a medial longitudinal section through a developing *arpc2* branch. Blue lines indicate cell wall thickness at branch locations marked by black arrows. **e**, Regression analysis of wall thickness as a function of distance from the branch tip in **d**. **f**, Wall thickness analyses in a population of *arpc2* trichome branches using propidium iodide fluorescence quantification. Values are mean ± s.d. ($n = 42$). **g**, **h**, Plots of perimeter length of the MDZ as a function of tip radius of curvature in wild type (**g**, $n = 16$) and *arpc2* (**h**, $n = 22$) trichomes. **i**, Centring of the MDZ relative to branch axis with 1 corresponding to a perfectly centred zone. Values are mean ± s.d. ($n = 19$ for WT, $n = 26$ for *arpc2*). *$P < 0.05$ (Student *t*-test). Scale bars, 10 μm in **a**, **b**, **f** and left panel in **d**; 100 nm in right panels in **d**.

data indicate that a wall thickness gradient exists with a sufficient magnitude to explain the observed proximo-distal strain gradients in this cell type (Supplementary Fig. 2h). Moreover, a combination of the measured thickness gradient with an elastic modulus gradient resulted in unrealistic growth predictions (Fig. 2f), such that the simultaneous existence of a significant matrix modulus gradient was excluded.

The optimized finite element model was used to simulate spatial stress and strain distributions of the young trichome branch (Fig. 2j,k). The cell radius and wall thickness both contribute to the expected increase in the distribution of stress and strain[28]. The sharp circular band of high stress near the branch apex is likely to be an overestimate due to the assumed abrupt transition from an anisotropic flank to isotropic tip in the finite element simulations. The simulated strain distribution of the wall was consistent with the experimental bead labelling data. Because of the known importance of actin for long-distance transport and secretion of new cell wall material, the model was also used to quantify the amount of new wall material needed to maintain thickness during cell expansion (Fig. 2l). It can be seen that there is a relatively shallow gradient of newly added material with higher values per element at the branch base. This result is expected because the base is initially thicker and more material is needed to maintain the initial thickness even though the strains are lower at the branch base. The simulation and wall marking data indicate that the mechanism of trichome morphogenesis bears little or no resemblance to tip growth, and instead is accomplished by highly regulated anisotropic diffuse growth in which spatial gradients in wall thickness and texture dictate the growth patterns.

Function of ARP2/3-generated actin networks

Microtubule-dependent microfibril patterning operates at cellular spatial scales to enable polarized branch elongation; however, the location and function of the most critical actin filament arrays are not known. In trichomes, ROP/RAC small GTPase signals generated by the ROP guanine nucleotide exchange factor (GEF) GEF SPIKE1 (SPK1)[29] operate on the heteromeric W/SRC[19,30] to positively regulate the actin filament nucleator ARP2/3[15,31]. In *arpc2*/*distorted2*, the

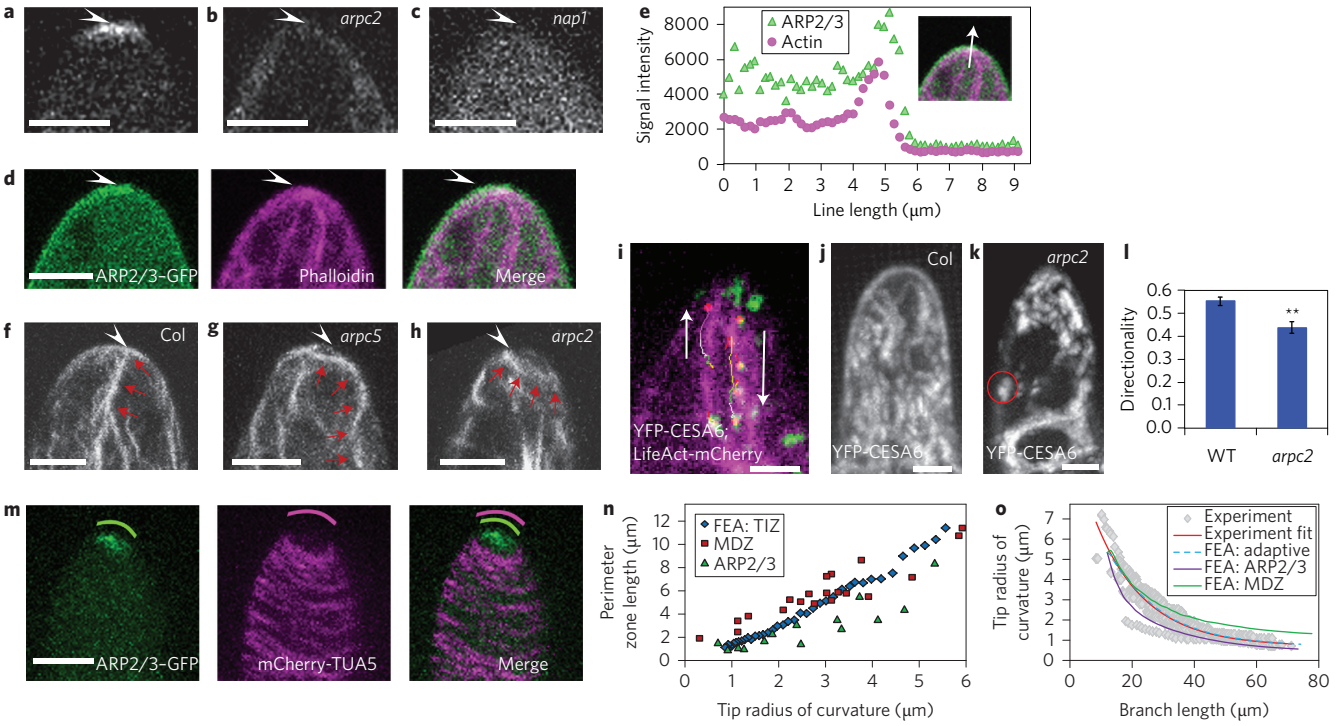

Figure 4 | ARP2/3 generates apical actin meshworks within the microtubule-depletion zone. a–c, ARP2/3 localization in the rescued line ARP2/3-GFP; *arpc5* (**a**); ARP2/3 localization in *arpc2* (**b**); ARP2/3 localization in the W/SRC mutant *nap1* (**c**). **d**, **e**, Co-localization of ARP2/3 and actin meshworks at the branch apex. ARP2/3 (green), phalloidin-labelled actin filaments (magenta), and merged images (**d**). Intensity plot of ARP2/3 and actin signals along the arrow shown in the inset of **e**. **f–h**, Apical actin meshworks labelled by phalloidin in wild type (**f**), and their absence in *arpc5* (**g**) and *arpc2* (**h**). Red arrows label actin bundles; arrowheads, branch apex. **i**, Particle tracking of Golgi (green) on actin bundles labelled with LifeAct-mCherry (magenta). Tracked Golgi are labelled red with a colorized path; arrows indicate the direction of the motility. **j**, **k**, Projections of Golgi motility over a 2 min interval in wild type (**j**) and *arpc2* (**k**). Red circle in **k** highlights Golgi with minimal movement. **l**, Directionality of Golgi movement is reduced in *arpc2*. Values are mean ± s.e. ($n > 150$), $^{**}P < 0.01$ (Wilcoxon test). **m**, ARP2/3 functions within the MDZ. ARP2/3 (green), microtubules (mCherry-TUA5, magenta) and merged images. Green and magenta lines indicate perimeter lengths of ARP2/3 signal and the MDZ. **n**, Geometry of the MDZ, ARP2/3 domain, and the optimal TIZ as a function of tip radius. The optimal TIZ was computed from **o**, using adaptive iteration. **o**, Finite element simulations using variable TIZ geometries derived from experimental data or a simulated optimal TIZ that generated the best fit to the observed tip refinement pattern. Scale bars, 5 μm.

ARP2/3 complex is disassembled[32], and following branch initiation the branch base and stalk were swollen (Fig. 3a). The terminal *arpc2* phenotype is a reduced branch length and severe cell swelling[33]. Time-lapse analyses of *arpc2* branches were technically challenging due to cell twisting and swelling. However, it was possible to obtain several time-lapse data sets (Supplementary Movie 2 and Fig. 3), albeit with some missing data points due to poor image quality. The growth of *arpc2* trichomes was inconsistent, switching repeatedly among paused, slow and normal growth rates (Fig. 3b,c). Because of the low success rate in imaging mutant branch growth, we had to resort to using visible cell wall protuberances to measure the local strain patterns instead of exogenously applied beads. The fast-growing *arpc2* branch shown in Fig. 3b did not have an increased strain rate in the distal regions of the branch (Supplementary Fig. 3a).

We next tested for a cell wall thickness gradient in developing *arpc2* branches. Unlike the wild type (Fig. 2g–i), the mutant branches lacked a clear tip to base thickness gradient based on the regression analyses of the TEM and propidium iodide image data (Fig. 3d–f and Supplementary Fig. 3b–d). The *arpc2* cell walls had a significantly increased thickness of 202.4 ± 11.8 nm compared with 109.7 ± 22.7 for the wild type. The wall was cellulose-rich, as observed in glancing TEM sections of the wall, with obvious fibrillar texture that was transverse to the branch axis and parallel to cortical microtubules that were present in the mutant (Supplementary Fig. 3e–g). Microtubule-based CESA insertion does not require an intact actin cytoskeleton[34]. In *aprc2* trichomes, growth and wall assembly are partially uncoupled, perhaps because cellulose synthesis is not coordinated with the delivery of wall matrix and/or wall loosening factors that enable normal wall strain behaviours. ARP2/3 has a second function at the branch tip based on the episodic and incomplete tip radius of curvature refinement detected in *arpc2* (Fig. 3c). To test for an effect of *arpc2* on the MDZ and the predicted TIZ, microtubule localization was analysed in a population of *arpc2* branches. Although the MDZ was clearly present in the mutant (Supplementary Fig. 3f), its size was uncoupled from the geometry of the cell tip and its centring at the branch apex was less accurate than the wild type (Fig. 3g–i). Therefore, ARP2/3 is not required to generate an MDZ, but may function either directly or indirectly with other ROP signalling pathways that locally destabilize microtubules[35,36], to position the microtubule free zone and modulate its size during tip refinement.

Our growth analyses suggested that ARP2/3 generates actin networks that have a global influence on the cell wall thickness gradient within a branch and a local influence on wall isotropy at the tip. In other systems, ARP2/3 and its generated actin networks localize at the leading edge of motile cells[37] and at sites of endocytic vesicle internalization in yeast[38–40]. However, the location of active ARP2/3 has not been clearly determined in any plant cell type. We therefore created a fully functional green fluorescent protein (GFP)-tagged version of the ARPC5 subunit (Supplementary Fig. 4a–h). ARPC5 functions in the context of an evolutionarily conserved ARP2/3 complex[32]; therefore, it is referred to as ARP2/3-GFP. ARP2/3-GFP was concentrated at the apex of

young, blunt-tipped (stage 4) trichome branches (Fig. 4a). ARP2/3 and the known W/SRC subunit BRICK1[41–43] were clustered at the apex in 28% and 66% of the stage 4 branches, respectively (Supplementary Table 2 and Supplementary Fig. 4i). The significance of the reversible recruitment of ARP2/3 to the branch apex could not be analysed because of photobleaching; however, when present at the tip ARP2/3 remained there for minutes. It is possible that BRICK1 and ARP2/3 clustering at the apex is episodic, and may correlate with growth rate fluctuations that were observed in time-lapse imaging studies (Supplementary Fig. 1). In pavement cells, a significant fraction of ARP2/3 appears to be inactive because its clustering on actin-bundle-associated organelles occurs even when the W/SRC is mutated[44]. In trichomes, tip-localized ARP2/3 corresponded to an active pool of the complex, because this localization was eliminated in *arpc2* (Fig. 4b), which leads to ARP2/3 disassembly[32] and in *nap1/gnarled*[19,45], which eliminates W/SRC-dependent positive regulation of fully assembled ARP2/3 (Fig. 4c). The importance of W/SRC for the local recruitment of ARP2/3, either from soluble or organelle-associated pools[32], may explain the more persistent localization of BRICK1 to the apex than ARP2/3. It is also possible that ARP2/3 functions more transiently at the apex as it cycles through rounds of activation and release.

Apical ARP2/3 was capable of generating actin filaments because it co-localized with cortical actin meshworks (Fig. 4d,e) and the tip-localized actin was ARP2/3 dependent (Fig. 4f–h). The presence of an apical actin meshwork was positively correlated with growth, because it was absent in *arpc2*, and only reduced in the *arpc5* (Supplementary Table 3), which has a more mild branch length phenotype than *arpc2*[42]. These genetic and co-localization results clearly demonstrate that the tip-localized ARP2/3 is active. The ARP2/3-generated cortical actin was related to core actin bundle positioning at the apex, because in 90% ($n = 20$) of the cases in which the apical meshwork was present, core actin bundles terminated at or near it (Fig. 4d,f). This result is consistent with previous reports of actin at the branch apex, and the known ARP2/3 dependence of actin bundle positioning within the core cytoplasm[13,17,19–21].

Based on the distorted trichome phenotype of MYOSIN XI mutants[46], acto-myosin-dependent organelle transport is a key component of growth control. Our time-lapse analyses of Golgi transport and actin bundle localization in wild-type trichomes did not detect an obviously organized flow pattern, which is typical of tip-growing cells; however, there was evidence for directional movement as a subset of Golgi staggered along actin bundle tracks (Fig. 4i, Supplementary Fig. 4j and Supplementary Movie 3). Frequent pauses, bidirectional flow along bundles with differing polarities, and exchange between the cortical and core cytoplasm efficiently circulated the Golgi throughout the branch as judged by projections of time-lapse images (Fig. 4j). Large numbers of motile Golgi were present in young *arpc2* branches; however, the directionality of their movement was reduced (Fig. 4l), and projections of time series images showed that Golgi motility was restricted to narrow trafficking lanes that were randomly positioned compared with the wild type (Fig. 4k and Supplementary Fig. 4j). Defects in the actin cytoskeleton organization have been linked to wall thickness and cell shape defects in hypocotyl epidermal cells[34]. Given the cell wall thickness defects in *arpc2*, ARP2/3 appears to operate at cellular scales by organizing an actin transport network that distributes secretory organelles throughout the cytoplasm so that wall assembly and growth are properly coupled. Certainly, additional levels of control at the plasma membrane, such as exocyst-dependent vesicle fusion[47], enable the cell to more precisely balance the secretion of matrix components with cellulose synthesis during morphogenesis.

ARP2/3-generated apical actin meshworks may also have a more local function to position the MDZ during growth. We found that the size of the ARP2/3-positive apical domain was strongly correlated with the tip geometry, and, based on two-colour live cell imaging, it was always positioned within the MDZ (Fig. 4m,n). An importance for modulation of the size of the TIZ was also demonstrated with the finite element model, because an improved fit with the experimental data was obtained when the regression lines from the MDZ and ARP2/3 localization data were used to couple the size of the TIZ and the radius of curvature during a simulation (Fig. 4o and Supplementary Table 4). ARP2/3-mediated modulation of the TIZ is a plausible mechanism to achieve tip radius refinement, because a perfect fit between the simulated and observed tip radius refinement could be generated by optimizing the size of the TIZ throughout the simulation (Fig. 4o).

To conclude, the polarized growth and developmental responses of plant cells frequently involve subcellular heterogeneity in the mechanical properties of the cell wall[3,48]. In cell types such as developing pavement cells[34,49] and tracheary elements[36], non-overlapping actin- and microtubule-based cortical domains can direct the local assembly of specialized cell walls. A major challenge is to understand the complex interactions between cytoskeletal patterning, wall mechanics and cell shape change. In this paper, we discover new mechanisms by which an apical actin meshwork and the microtubule cytoskeleton cooperate to organize the cytoplasm to pattern the cell wall and shape change. A defined threshold of microfibril alignment and a wall thickness gradient along the branch length were identified as key parameters for polarized diffuse growth using a validated finite element computational model. An ARP2/3-generated actin meshwork influences wall thickness gradients by positioning a network of core actin bundles that organize a bidirectional trafficking system for distributed secretion. The thickness gradient introduces an apical bias to elongation and promotes rapid cell expansion. Tip refinement is another critical feature during leaf trichome and cotton fibre[50] development, and we find this change is mediated by the geometry of an isotropic zone at the branch apex. ARP2/3 is activated within an apical MDZ with predicted isotropic cell wall character to mediate smooth tip refinement during growth. It is possible that intracellular signalling and the polarization of cytoskeletal and membrane domains are sufficient to control local wall properties during tip refinement[36]. Alternatively, mechanical properties of the cell wall may feed back on intracellular pathways to coordinate events in the cytoplasm with the status of the extracellular matrix[34]. The W/SRC complex transmits activating ROP GTPase signals to ARP2/3[29]. Given the importance of ARP2/3 for the morphogenesis of nearly all epidermal cell types, this work may serve as a general model to understand how nanometre-sized, actin filament-nucleating machines can control intracellular organization and cell wall assembly at the micrometre scale of cells.

Methods

Plant materials, growth conditions, and trichome stage definitions. *Arabidopsis* ecotype Col-0 was used as the wild type. The *arpc5/crk-1*[16], *arpc2/dis2-1*[33] and *nap1/grl-6*[45] alleles have been described previously. The plant materials for fluorescence imaging were grown on half-strength Murashige and Skoog medium with 1% sucrose and 0.8% Bacto agar under continuous illumination at 22°C. Reflected light microscopy and TEM imaging employed soil-grown plants with continuous illumination at 22°C. For all experiments, young trichomes are defined as stage 4 trichomes having blunt tips and branch lengths less than 50 µm. Staging distorted mutant trichomes is complicated because the branches remain blunt and their final length is reduced. Time-lapse analyses of *arpc2* trichomes showed that if the total cell height was less than 50 µm and branch length was less than 30 µm, the branches were likely to elongate. Therefore, all imaging and measurements of mutant branches utilized cells that fell at or below these size classes.

Reflected light microscopy. For time-lapse imaging of trichome growth using reflected light microscopy, plants were imaged at either 3 days after germination (DAG) or 11–15 DAG. White light from a metal halogen lamp was filtered through a 525/50 (Chroma) band-pass filter then directed to the sample using a 50% transmissive beamsplitter (Chroma), which allowed reflected light to be directed to the detector. Images were collected using a 50× LU-Apo 0.55 numerical aperture (NA) long working distance objective lens and a Coolsnap HQ camera (Photometrics) mounted on a Nikon 80i microscope. Stacks were captured at 5, 10

or 15 min intervals using a *z*-step size of 0.5 μm. Images of mature trichome tips for the wild type and *arpc2* mutant were captured under bright-field illumination using a 60× PlanApo 1.2 NA water objective lens. Devices were controlled using Slidebook software version 5.5 (Intelligent Imaging Innovations).

Bead labelling and fluorescence microscopy. Deep red fluorescent polystyrene beads (0.17 μm; Molecular Probes) were applied to newly emerged leaves of 10–13 DAG seedlings. The seedlings were air dried for 1 h and gently rinsed with water to remove unbound beads before mounting. A whole seedling with agar containing growth media was transferred to our homemade gas-permeable chamber, which was constructed using a microscope slide and a cover slip with 2.5 mm silicon isolator (JRT-SA2-2.5, Grace Bio-Labs) between them. The rare stage 4 trichomes between 15 and 34 μm in length with high and uniform bead coverage were selected for further analysis. In chambered slides, the branch elongation rates varied from 1.7 to 3.4 μm h^{-1}, and were similar to those observed for soil grown plants. For detailed information on all other fluorescent probes and the configuration of the spinning disc imaging platform please refer to the Supplementary Information.

Finite element modelling. The finite element model of a trichome branch was created using Abaqus 6.11. The trichome branch was modelled as an axisymmetric shell reservoir under constant hydrostatic pressure representing turgor pressure (Supplementary Fig. 5). Effects of material and thickness gradients were studied by subdividing the shell longitudinally (from the tip to the base) into several sections. The influence of tip isotropy on tip refinement was investigated by creating isotropic regions of variable size near the branch tip, namely the TIZ. A specific hyperelastic anisotropic constitutive material model was chosen[24] because of its relevance to a fibre-reinforced plant cell wall. The effect of the model parameters on overall growth shape of the trichome branch was studied to understand their specific influence on growth behaviour. A standard linear solid (SLS) viscoelastic material was assumed to represent the time-dependent (viscoelastic) behaviour of the wall with initial values taken from pavement cell measurements[51]. Growth was modelled as a sequence of several steps: expanding the branch cell wall due to turgor pressure, using this deformed geometry into the next simulation run, redefining sections and resetting initial thicknesses values representing synthesis of new material (similar to previous work[4] for polar growth of pollen tubes). Each loading step (defined as one "growth cycle") concluded when the wall was fully relaxed and 30–100 growth cycles were needed to achieve final trichome lengths representative of experiments. Optimization of the TIZ size (an adaptive technique) was performed until it was within 2% of the experimental tip radius of curvature (3–6 repetitions were needed for convergence). Several methods were developed to connect the simulation results with the experiments to determine the model parameters. For a more detailed description of the finite element model and its parameters please refer to the Supplemental Information.

Received 31 October 2014; accepted 23 January 2015; published 2 March 2015

References

1. Rodriguez, O. C. *et al.* Conserved microtubule-actin interactions in cell movement and morphogenesis. *Nature Cell Biol.* **5,** 599–609 (2003).
2. Smith, L. G. & Oppenheimer, D. G. Spatial control of cell expansion by the plant cytoskeleton. *Annu. Rev. Cell Dev. Biol.* **21,** 271–295 (2005).
3. Baskin, T. I. Anisotropic expansion of the plant cell wall. *Annu. Rev. Cell Dev. Biol.* **21,** 203–222 (2005).
4. Fayant, P. *et al.* Finite element model of polar growth in pollen tubes. *Plant Cell* **22,** 2579–2593 (2010).
5. Szymanski, D. B. & Cosgrove, D. J. Dynamic coordination of cytoskeletal and cell wall systems during plant cell morphogenesis. *Curr. Biol.* **19,** R800–811 (2009).
6. Zhang, C., Halsey, L. E. & Szymanski, D. B. The development and geometry of shape change in *Arabidopsis thaliana* cotyledon pavement cells. *BMC Plant Biol.* **11,** 27 (2011).
7. Andriankaja, M. *et al.* Exit from proliferation during leaf development in *Arabidopsis thaliana*: a not-so-gradual process. *Dev. Cell* **22,** 64–78 (2012).
8. Walter, A., Silk, W. K. & Schurr, U. Environmental effects on spatial and temporal patterns of leaf and root growth. *Annu. Rev. Plant Biol.* **60,** 279–304 (2009).
9. Paredez, A. R., Somerville, C. R. & Ehrhardt, D. W. Visualization of cellulose synthase demonstrates functional association with microtubules. *Science* **312,** 1491–1495 (2006).
10. Fujita, M. *et al.* The anisotropy1 D604N mutation in the *Arabidopsis* cellulose synthase1 catalytic domain reduces cell wall crystallinity and the velocity of cellulose synthase complexes. *Plant Physiol.* **162** (2013).
11. Mauricio, R. Costs of resistance to natural enemies in field populations of the annual plant *Arabidopsis thaliana*. *Am. Nat.* **151,** 20–28 (1998).
12. Tiwari, S. C. & Wilkins, T. A. Cotton (*Gossypium hirsutum*) seed trichomes expand via diffuse growing mechanism. *Can. J. Bot.* **73,** 746–757 (1995).
13. Szymanski, D. B., Marks, M. D. & Wick, S. M. Organized F-actin is essential for normal trichome morphogenesis in *Arabidopsis*. *Plant Cell* **11,** 2331–2347 (1999).
14. Mathur, J., Spielhofer, P., Kost, B. & Chua, N. The actin cytoskeleton is required to elaborate and maintain spatial patterning during trichome cell morphogenesis in *Arabidopsis thaliana*. *Development* **126,** 5559–5568 (1999).
15. Zhang, C. *et al. Arabidopsis SCAR*s function interchangeably to meet actin-related protein 2/3 activation thresholds during morphogenesis. *Plant Cell* **20,** 995–1011 (2008).
16. Mathur, J. *et al.* Arabidopsis CROOKED encodes for the smallest subunit of the ARP2/3 complex and controls cell shape by region specific fine F-actin formation. *Development* **130,** 3137–3146 (2003).
17. Le, J., El-Assal, S. E., Basu, D., Saad, M. E. & Szymanski, D. B. Requirements for *Arabidopsis ATARP2* and *ATARP3* during epidermal development. *Curr. Biol.* **13,** 1341–1347 (2003).
18. Yanagisawa, M., Zhang, C. & Szymanski, D. B. ARP2/3-dependent growth in the plant kingdom: SCARs for life. *Front. Plant Sci.* **4,** 166 (2013).
19. Deeks, M. J., Kaloriti, D., Davies, B., Malho, R. & Hussey, P. J. *Arabidopsis* NAP1 is essential for ARP2/3-dependent trichome morphogenesis. *Curr. Biol.* **14,** 1410–1414 (2004).
20. Zhang, X., Dyachok, J., Krishnakumar, S., Smith, L. G. & Oppenheimer, D. G. IRREGULAR TRICHOME BRANCH1 in *Arabidopsis* encodes a plant homolog of the actin-related protein2/3 complex activator Scar/WAVE that regulates actin and microtubule organization. *Plant Cell* **17,** 2314–2326 (2005).
21. Sambade, A., Findlay, K., Schaffner, A. R., Lloyd, C. W. & Buschmann, H. Actin-dependent and -independent functions of cortical microtubules in the differentiation of *Arabidopsis* leaf trichomes. *Plant Cell* **26** (2014).
22. Schwab, B. *et al.* Regulation of cell expansion by the *DISTORTED* genes in *Arabidopsis thaliana*: actin controls the spatial organization of microtubules. *Mol. Genet. Genome* **269,** 350–360 (2003).
23. Beilstein, M. & Szymanski, D. in *The Plant Cytoskeleton in Cell Differentiation and Development* (ed. Hussey, P.) 265–289 (Blackwell, 2004).
24. Gasser, T. C., Ogden, R. W. & Holzapfel, G. A. Hyperelastic modelling of arterial layers with distributed collagen fibre orientations. *J. R. Soc. Interface* **3,** 15–35 (2006).
25. Huang, R., Becker, A. A. & Jones, I. A. Modelling cell wall growth using a fibre-reinforced hyperelastic-viscoplastic constitutive law. *J. Mech. Phys. Solids* **60,** 750–783 (2012).
26. McKenna, S. T. *et al.* Exocytosis precedes and predicts the increase in growth in oscillating pollen tubes. *Plant Cell* **21,** 3026–3040 (2009).
27. Rounds, C. M., Lubeck, E., Hepler, P. K. & Winship, L. J. Propidium iodide competes with Ca(2+) to label pectin in pollen tubes and Arabidopsis root hairs. *Plant Physiol.* **157,** 175–187 (2011).
28. Timoshenko, S. *Strength of materials* (New York, 1930).
29. Basu, D., Le, J., Zakharova, T., Mallery, E. L. & Szymanski, D. B. A SPIKE1 signaling complex controls actin-dependent cell morphogenesis through the heteromeric WAVE and ARP2/3 complexes. *Proc. Natl Acad. Sci. USA* **105,** 4044–4049 (2008).
30. Basu, D., El-Assal, S. E., Le, J., Mallery, E. L. & Szymanski, D. B. Interchangeable functions of *Arabidopsis* PIROGI and the human WAVE complex subunit SRA1 during leaf epidermal development. *Development* **131,** 4345–4355 (2004).
31. Basu, D. *et al.* DISTORTED3/SCAR2 is a putative *Arabidopsis* WAVE complex subunit that activates the Arp2/3 complex and is required for epidermal morphogenesis. *Plant Cell* **17,** 502–524 (2005).
32. Kotchoni, S. O. *et al.* The association of the *Arabidopsis* actin-related protein (ARP) 2/3 complex with cell membranes is linked to its assembly status, but not its activation. *Plant Physiol.* **151,** 2095–2109 (2009).
33. El-Assal, S. E., Le, J., Basu, D., Mallery, E. L. & Szymanski, D. B. *DISTORTED2* encodes an ARPC2 subunit of the putative *Arabidopsis* ARP2/3 complex. *Plant J.* **38,** 526–538 (2004).
34. Sampathkumar, A. *et al.* Patterning and lifetime of plasma membrane-localized cellulose synthase is dependent on actin organization in *Arabidopsis* interphase cells. *Plant Physiol.* **162,** 675–688 (2013).
35. Lu, L., Lee, Y.-R. J., Pan, R., Maloof, J. N. & Liu, B. An internal motor kinesin is associated with the Golgi apparatus and plays a role in trichome morphogenesis in *Arabidopsis*. *Mol. Biol. Cell* **16,** 811–823 (2005).
36. Oda, Y. & Fukuda, H. Initiation of cell wall pattern by a Rho- and microtubule-driven symmetry breaking. *Science* **337,** 1333–1336 (2012).
37. Pollard, T. D. & Borisy, G. G. Cellular motility driven by assembly and disassembly of actin filaments. *Cell* **112,** 453–465 (2003).
38. McCollum, D., Feoktistova, A., Morphew, M., Balasubramanian, M. & Gould, K. L. The *Schizosaccharomyces pombe* actin-related protein, Arp3, is a component of the cortical actin cytoskeleton and interacts with profilin. *EMBO J.* **15,** 6438–6446 (1996).
39. Winter, D., Podtelejnikov, A. V., Mann, M. & Li, R. The complex containing actin-related proteins Arp2 and Arp3 is required for the motility and integrity of yeast actin patches. *Curr. Biol.* **7,** 519–529 (1997).

40. Evangelista, M., Pruyne, D., Amberg, D. C., Boone, C. & Bretscher, A. Formins direct Arp2/3-independent actin filament assembly to polarize cell growth in yeast. *Nature Cell Biol.* **4,** 260–269 (2002).
41. Le, J., Mallery, E. L., Zhang, C., Brankle, S. & Szymanski, D. B. *Arabidopsis* BRICK1/HSPC300 is an essential WAVE-complex subunit that selectively stabilizes the Arp2/3 activator SCAR2. *Curr. Biol.* **16,** 895–901 (2006).
42. Djakovic, S., Dyachok, J., Burke, M., Frank, M. J. & Smith, L. G. BRICK1/HSPC300 functions with SCAR and the ARP2/3 complex to regulate epidermal cell shape in *Arabidopsis*. *Development* **133,** 1091–1100 (2006).
43. Dyachok, J. *et al.* Plasma membrane-associated SCAR complex subunits promote cortical F-actin accumulation and normal growth characteristics in *Arabidopsis* roots. *Mol. Plant* **1,** 990–1006 (2008).
44. Zhang, C., Mallery, E. & Szymanski, D. B. ARP2/3 localization in Arabidopsis leaf pavement cells: a diversity of intracellular pools and cytoskeletal interactions. *Front. Plant Biol.* **4,** 1–16 (2013).
45. El-Assal, S. E., Le, J., Basu, D., Mallery, E. L. & Szymanski, D. B. Arabidopsis *GNARLED* encodes a NAP125 homologue that positively regulates ARP2/3. *Curr. Biol.* **14,** 1405–1409 (2004).
46. Ojangu, E. L. *et al.* Myosins XI-K, XI-1, and XI-2 are required for development of pavement cells, trichomes, and stigmatic papillae in *Arabidopsis*. *BMC Plant Biol.* **12,** 81 (2012).
47. Fendrych, M. *et al.* The *Arabidopsis* exocyst complex is involved in cytokinesis and cell plate maturation. *Plant Cell* **22,** 3053–3065 (2010).
48. Boudaoud, A. An introduction to the mechanics of morphogenesis for plant biologists. *Trends Plant Sci.* **15,** 353–360 (2010).
49. Szymanski, D. B. The kinematics and mechanics of leaf expansion: new pieces to the Arabidopsis puzzle. *Curr. Opin. Plant Biol.* **22C,** 141–148 (2014).
50. Butterworth, K. M., Adams, D. C., Horner, H. T. & Wendel, J. F. Initiation and early development of fiber in wild and cultivated cotton. *Int. J. Plant Sci.* **170,** 561–574 (2009).
51. Forouzesh, E., Goel, A., Mackenzie, S. A. & Turner, J. A. *In vivo* extraction of Arabidopsis cell turgor pressure using nanoindentation in conjunction with finite element modeling. *Plant J.* **73,** 509–520 (2013).

Acknowledgements

We thank David Umulis for helpful discussions. Thanks to Adam Fessenden for reflected light time-lapse imaging. We also thank Chia-Ping Huang and the Purdue Life Science Microscopy Facility for their expert assistance. This research was supported by NSF Grant IOS Grant No. 1249652 to D.B.S and J.A.T. and NSF MCB Grant No. 1121893 to D.B.S.

Author contributions

All authors participated in the experimental design, data collection, data analysis and manuscript preparation. D.S. conceived the project. J.T. and A.D. developed the finite element models. S.B. did the reflected light and TEM analyses. E.M. created the ARP2/3–GFP live-cell probe. M.Y. conducted all other wet laboratory experiments.

Additional information

Supplementary information is available online. Reprints and permissions information is available online at www.nature.com/reprints. Correspondence and requests for materials should be addressed to D.B.S.

Competing interests

The authors declare no competing financial interests.